Sustainable
Energy & Fuels

ROYAL SOCIETY
OF CHEMISTRY

PAPER

View Article Online
View Journal | View Issue

Check for updates

Cite this: *Sustainable Energy Fuels*, 2024, **8**, 2180

Engineering of the perovskite/electron-transporting layer interface with transition metal chalcogenides for improving the performance of inverted perovskite solar cells†

Dimitris Tsikritzis,[ab] Konstantinos Chatzimanolis,[a] Nikolaos Tzoganakis,[a] Konstantinos Rogdakis,[ab] Marilena Isabella Zappia,[c] Beatriz Martín-García,[def] Ahmad Bagheri,[cd] Hossein Beydaghi,[c] Lukáš Děkanovský,[g] Zdeněk Sofer,[g] Sebastiano Bellani,[c] Francesco Bonaccorso[cd] and Emmanuel Kymakis[ab]

Layered two-dimensional (2D) transition-metal chalcogenides (TMCs) attract substantial interest across multiple disciplines due to their unique properties. In perovskite solar cells (PSCs), researchers have extensively explored the integration of 2D TMCs to enhance device power conversion efficiency (PCE) and stability. However, there is a research gap in understanding their impact on inverted (p–i–n) PSCs, especially at the perovskite/electron-transporting layer (ETL) interface. This study addresses this gap by investigating the effect of inserting InSe, $MoSe_2$, and SnS_2 nanosheets at the perovskite/ETL interface in inverted PSCs. The introduction of 2D TMC interlayers induces a downward shift in perovskite energy levels, optimizing the energy level alignment at the perovskite/ETL interface and substantially increasing the PCE. The SnS_2-incorporating PSCs exhibit the highest relative improvement of 5.05% (InSe and $MoSe_2$ nanosheets yield 3.37% and 2.5% PCE increase, respectively). This enhancement results in an absolute PCE of 18.5% with a fill factor exceeding 82%. Furthermore, the incorporation of InSe nanosheets eliminates the burn-in phase enhancing the long-term stability (T_{70} of 250 h) of unencapsulated devices. This study underscores the significant improvement in PSCs' PCE and stability by selectively incorporating suitable TMCs at the perovskite/ETL interface. This research offers insights into the potential role of TMCs in advancing PSCs.

Received 9th February 2024
Accepted 3rd April 2024

DOI: 10.1039/d4se00212a

rsc.li/sustainable-energy

Introduction

Transition metal chalcogenides (TMCs) represent a highly promising class of materials with a wide range of applications. These materials exhibit exceptional optical, electrical, catalytic, and mechanical properties, making them suitable for numerous fields, including batteries,[1,2] supercapacitors,[3], (photo)catalysis,[4–8], (photo)transistors[9–11] and other optoelectronic devices.[12–17] One feature of TMCs is their band gap tunability, which makes them ideal for adjustable light absorption, *e.g.*, serving as the photoactive layer in photovoltaic applications. However, photovoltaic devices using TMC-based photoactive layers currently exhibit insufficient power conversion efficiency (PCE) just above 5%.[18,19] When integrated with other photoactive layers as interlayers or additives, TMCs have been reported to enhance the performance of solar cells by finely tuning specific device characteristics, ultimately improving the overall performance.[20] For instance, MoS_2 has been successfully integrated into both Si-based[21,22] and organic solar cells,[23] improving significantly the cell performance. The role of TMCs depends specifically on photovoltaic technologies, for each of which a systematic investigation of the role of TMCs is required for reliable advancements in this field.[24]

In this context, the incorporation of TMCs, typically in their two-dimensional (2D) forms (*i.e.*, nanosheets), in perovskite solar cells (PSCs) has been investigated in various studies.[24–26] In particular, MoS_2 was deposited on the perovskite in normal (n–i–

---

[a] *Department of Electrical & Computer Engineering, Hellenic Mediterranean University (HMU), Heraklion 71410, Crete, Greece. E-mail: kymakis@hmu.gr*

[b] *Institute of Emerging Technologies (i-EMERGE) of HMU Research Center, Heraklion 71410, Crete, Greece*

[c] *BeDimensional S.p.A., Via Lungotorrente Secca 30R, 16163 Genova, Italy*

[d] *Graphene Labs, Istituto Italiano di Tecnologia, Via Morego, 30, 16163, Genova, Italy*

[e] *CIC NanoGUNE BRTA, 20018 Donostia-San Sebastián, Basque Country, Spain*

[f] *IKERBASQUE, Basque Foundation for Science, 48009 Bilbao, Spain*

[g] *Department of Inorganic Chemistry, University of Chemistry and Technology Prague, Technická 5, 166 28 Prague 6, Czech Republic*

† Electronic supplementary information (ESI) available: Material synthesis, exfoliation, and characterization, PSC fabrication and characterization. Moreover, in the supplementary material are presented the TEM statistical analysis, XPS spectra, SEM images, box charts of PSC photovoltaic parameters, W_F measurements, and APS measurements. See DOI: https://doi.org/10.1039/d4se00212a

p) PSCs, acting as an interlayer between the perovskite and the hole-transporting layer (HTL) to enhance the device PCE and stability by improving the hole extraction processes and offering a physical barrier against ion migration from the metal contact to the perovskite and *vice versa*.[27–29] In a similar study, $MoSe_2$ nanosheets were also screened together with MoS_2 ones to form thin interlayers between the perovskite and the HTL in normal PSC structures, enhancing the performance of reference devices.[30–32] MoS_2 was also used in combination with graphene-incorporating electron transporting layers (ETLs) and MXene-incorporating perovskites, testifying the effectiveness of 2D material interface engineering.[33,34] Also, TMCs have been proposed as charge-transporting layers to completely replace conventional materials of PSCs.[24,35] Specifically, MoS_2 and WS_2 were used as HTLs in inverted PSCs showing similar PCEs to the references based on poly(3,4-ethylenedioxythiophene):poly(styrenesulfonate) (PEDOT:PSS).[36,37] SnS_2 was used as the ETL in PSCs, improving the PCE up to 20%.[38] Despite its n-type behavior, $MoSe_2$ was used as an HTL in an inverted PSC,[39] showing a high PCE of 18%. The mixing of PEDOT:PSS with MoS_2, as well as other dichalcogenides, was used to increase the PCE of inverted PSCs.[40–42] Dichalcogenides, including MoS_2, but also other TMCs, have also been proposed to modify the electron-transporting layer (ETL)/metal electrode interface, aiming at creating favorable energy level alignments to efficiently collect photogenerated electrons.[26,43–45]

Despite the tremendous progress recently achieved by incorporating MoS_2 in PSCs, including the realization of the world's first perovskite solar farm operating for several months,[46] other representative TMCs for photovoltaic applications, based on the above consideration, are SnS_2, $MoSe_2$, as well as monochalcogenides, *e.g.*, InSe.[24] While MoS_2 is mainly used to improve the hole extraction efficiency in n–i–p PSCs, there are other TMCs that may play a relevant role in promoting the electron extraction from the perovskite to the current collectors. In particular, SnS_2 is an n-type layered semiconductor with a tunable band gap ranging from 2.1 to 3.4 eV, depending on the number of its layers. In its bulk form, SnS_2 has already been established in photovoltaic applications.[47] Meanwhile, the exfoliation of SnS_2 into 2D few-layer nanosheets has been achieved through both chemical[48] and physical methods.[49] Extensive characterization of SnS_2 has revealed that its monolayer possesses an indirect bandgap equal to 2.033 eV, while its field-effect transistor (FET) mobility was estimated to be in the range of 5 $cm^2\ V^{-1}\ s^{-1}$ to 250 $cm^2\ V^{-1}\ s^{-1}$,[50] enabling the realization of ultrathin FETs and logic gates.[49] Also, SnS_2 shows a high electron density of $\sim 6 \times 10^{-19}\ cm^{-3}$,[48] justifying its use as an effective dopant for $PC_{70}BM$ in inverted PSCs.[51] In this context, the high conductivity of 2D SnS_2 has been leveraged for the fabrication of ultra-thin ETLs in PSCs.[38,52] The valence band maximum (VB) and conduction band minimum (CB) of 2D SnS_2 have been estimated through ultraviolet photoelectron spectroscopy (UPS) to be −6.54 and −4.24 eV, respectively, indicating their potential ability to collect electrons from common perovskite active layers.[38]

$MoSe_2$ shows a similar structure to that of MoS_2 (2H phase). $MoSe_2$ is a semiconductor with an indirect band gap of 1.41 eV.[53] However, few-layer $MoSe_2$ exhibits a direct band gap of 1.58 eV (ref. 53 and 54) and a FET electron mobility of 50–250 $cm^2\ V^{-1}\ s^{-1}$.[55] Thin-films of 2D $MoSe_2$ have been used in photovoltaics,[56,57] catalysis for the hydrogen evolution reaction,[58,59] and energy storage systems.[60,61]

Finally, InSe is a III–VI layered compound made of stacked quaternary layers of Se–In–In–Se atoms that are held together by van der Waals interactions. Consequently, bulk InSe can be exfoliated into 2D forms by means of various methods, including scalable liquid-phase exfoliation (LPE) techniques.[62–64] InSe is generally considered as an n-type semiconductor and it was shown through experimental and theoretical studies that a band gap transition from direct to indirect occurs when InSe layer thickness reduces below 6 nm.[65] Also, its bandgap can increase from ∼1.2 eV for the bulk to 1.4 eV for few-layers InSe[66] and up to 2.1 eV for a monolayer of InSe.[67] The electron affinity was found to be −4.55 eV and the work function (W_F) to be 5.1 eV for bulk InSe.[68] The Hall mobility of InSe nanosheets was estimated to be $\sim 10^3\ cm^2\ V^{-1}\ s^{-1}$ at room temperature (RT)[69] and the carrier density was measured to be $\sim 10^{13}\ cm^{-2}$.[70] Pioneering studies also demonstrated n-type FETs based on 2D InSe, with an electron mobility at room temperature (RT) on the order of $10^3\ cm^2\ V^{-1}\ s^{-1}$.[71] This electron mobility is higher than those achieved by other high mobility 2D semiconducting materials, including MoS_2. Based on its properties, 2D InSe has been used in photovoltaic devices,[72,73] as well as for (photo)electrochemical water splitting reactions,[64] photodetectors,[63,74] sensors,[75] thermoelectric devices,[76] and spintronic devices.[77]

Overall, the above discussed TMCs represent interesting 2D materials for the engineering of the perovskite/ETL interface, aiming at improving the device PCE. Most studies on incorporating TMCs in PSCs have been focused on the optimization of the perovskite/HTL interface. To the best of our knowledge, there is no systematic work on engineering the perovskite/ETL interface with TMCs. In this study, we aim to fill this research gap by studying representative TMCs, *i.e.*, SnS_2, $MoSe_2$ and InSe, to optimize the perovskite/ETL interface in inverted PSCs. Selected TMCs, exfoliated through LPE, were deposited over the perovskite layer using solution processing, ensuring the scalability and industrialization feasibility of our interface engineering approach. The insertion of TMCs between the perovskite layer and the $PC_{70}BM$ effectively aligns the energy levels of the materials, enabling an efficient electron extraction from the perovskite to the current collector. This research aims to contribute to the extension of current 2D material interface engineering strategies to PSCs, providing new insights into the application of TMCs in inverted PSCs. The findings of this study have implications on the development of high-performance solar cells and can boost the utilization of TMCs in large-scale solar energy production, as already demonstrated for 2D MoS_2.[46]

Results

The methods of bulk TMC synthesis and exfoliation, and those for characterization of the exfoliated TMCs, are reported in the

ESI.† In particular, bulk 2H-$MoSe_2$, 2H-SnS_2 and β-InSe were exfoliated through ultrasonication-assisted LPE in isopropyl alcohol (IPA),[78,79] followed by sedimentation-based separation (SBS) to remove unexfoliated crystals from the exfoliated material.[59,80] Fig. 1a, d and g show the transmission electron microscopy (TEM) images of representative nanosheets of $MoSe_2$, SnS_2 and InSe, respectively. Fig. S1† reports the statistical analysis of the lateral size of the nanosheets. The lateral size data approximately follow log-normal distributions, with modes of 52.9 nm, 99.1 nm, and 143.9 nm for $MoSe_2$, SnS_2 and InSe nanosheets, respectively. Fig. 1b, e and h report the XRD patterns recorded for $MoSe_2$, SnS_2 and InSe nanosheets, respectively, comparing them with those measured for the bulk counterparts. The positions of the diffraction peaks of the exfoliated samples resemble those of the bulk counterparts, well-matching with the patterns of their hexagonal phases, *i.e.*, 2H-$MoSe_2$, $P\bar{6}m2$ space group, JCPDS card no. 029-0914; 2H-SnS_2, $P6_3mc$ space group, JCPDS card no. 023-0677; β-InSe structure, $P6_3/mmc$ space group, JCPDS card no. 034-1431. Bulk crystals show the diffraction peaks belonging to the {00l} family, which means that they are aligned along the (001) plane perpendicular to the *c* axis. Compared to the bulk materials, $MoSe_2$ and InSe nanosheets exhibit additional XRD peaks, likely due to their disordered arrangements. SnS_2 nanosheets, instead, preserve a placement perpendicular to their *c* axis. The broadening of the XRD peaks in the exfoliated materials indicate that their crystal sizes decreased after the LPE process. Fig. 1c, f and i report the Raman spectra of the bulk and exfoliated materials, exhibiting the characteristic Raman modes expected for each material by the group theory.[81–83] In $MoSe_2$ nanosheets, the redshift of the A_{1g} peak compared to the same peak of the bulk counterpart is explained by the softening of the

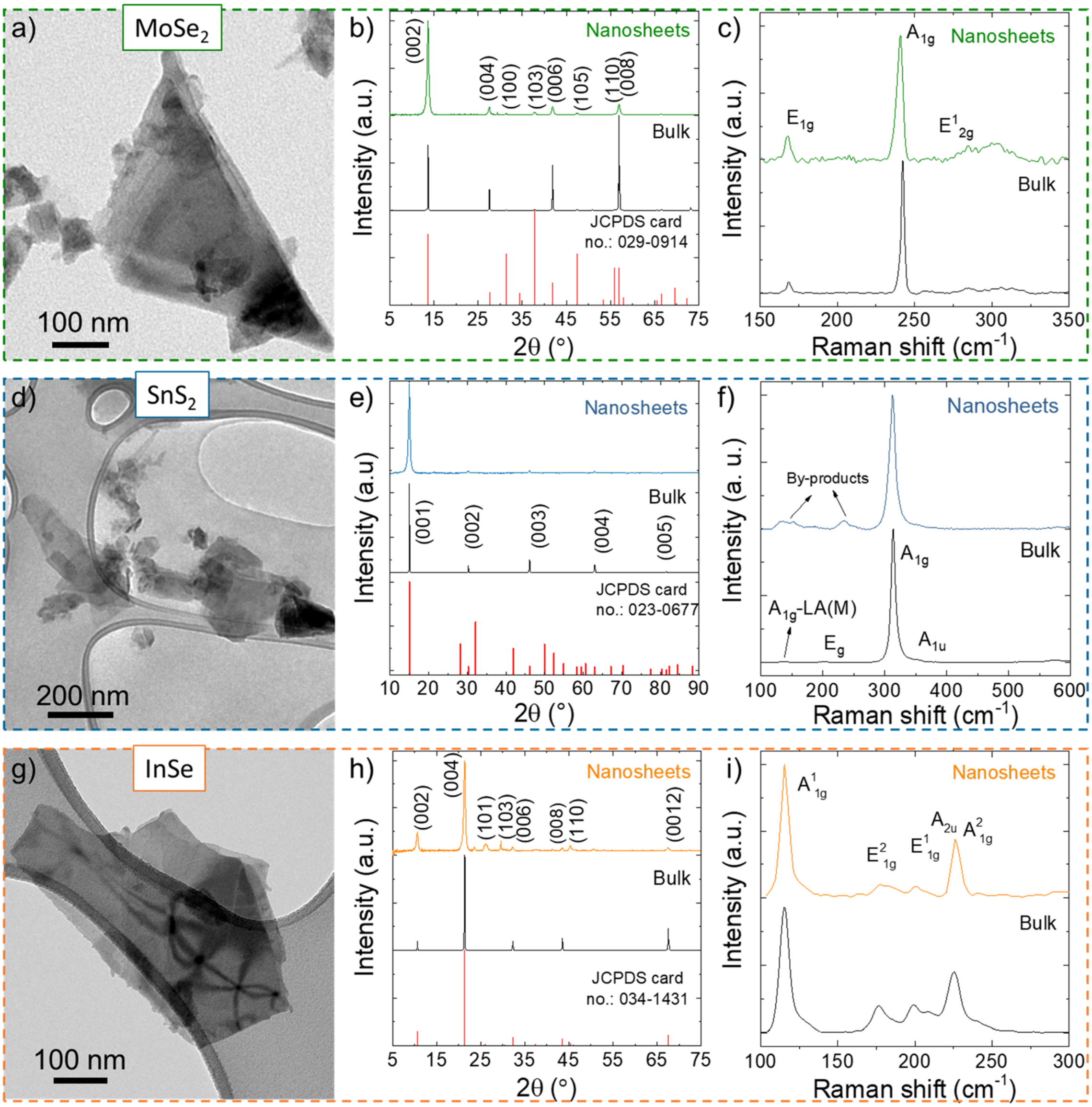

Fig. 1 TEM images, XRD patterns and Raman spectra measured for (a–c) $MoSe_2$, (d–f) SnS_2 and (g–i) InSe nanosheets. The XRD patterns and Raman spectra of bulk counterparts are also shown for comparison.

vibrational mode with decreasing the crystal thickness.[84,85] The Raman spectrum of bulk SnS_2 shows two phonon modes at ∼313 cm^{-1} (A_{1g}) and ∼203 cm^{-1} (E_g), as well as a weak two-phonon scattering signal of A_{1g}-LA (M) (Fig. 1f).[86] After exfoliation, additional peaks appear and are likely associated with by-products, *e.g.*, oxides.[87] Finally, bulk and exfoliated InSe exhibit various Raman peaks at similar positions, *i.e.*, A^1_{1g} at ∼116 cm^{-1}, E^2_{1g} at ∼177 cm^{-1}, E^1_{2g} at ∼199 cm^{-1}, A_{2u} at ∼208 cm^{-1}, and A^2_{1g} at ∼227 cm^{-1}, which is consistent with previous studies.[63,64]

The deposition of TMC nanosheets was carried out by spin coating their dispersion (formulated in chlorobenzene) onto the perovskite layer. Successive spin coating steps were applied to optimize the interlayer of TMC nanosheets at the perovskite/$PC_{70}BM$ interface. The formation of ultrathin 2D TMC films on the surface of the perovskites was assessed through X-ray photoelectron spectroscopy (XPS) and scanning electron microscopy (SEM) measurements. As shown in Fig. S2,† the 3d In, Mo, and Sn XPS spectra, acquired on the perovskite surfaces treated with 2D TMCs, confirm the presence of InSe, $MoSe_2$ and SnS_2 nanosheets, respectively. Fig. S3† presents top-view SEM images of the perovskite surface treated with 2D TMCs. The images show scattered TMC nanosheets atop the perovskite surface, without the presence of large material aggregates. Importantly, the few-layer nature of the exfoliated TMCs permits nanometer-thick interlayers to be obtained without resulting in significant changes of the surface topography of the underlying perovskite film.

The effect of the 2D TMC interlayers between the perovskite and $PC_{70}BM$ layers was evaluated by measuring the device performance estimated through the analysis of their *J*–*V* curves under 1 sun illumination. Fig. S4–S6† report the statistical analysis of the photovoltaic parameters, *i.e.*, PCE, open circuit voltage (V_{oc}), fill factor (FF) and short circuit current (J_{sc}), for the investigated devices, produced with different 2D TMC interlayers and by varying the number of successive spin coating steps used for the deposition of 2D TMCs atop the perovskite. These data indicate that the number of spin coating steps has a significant impact on the final photovoltaic parameters of the devices. Specifically, exceeding two spin coating steps has a detrimental effect on the device performance. This negative effect is likely associated with the excessive exposure of the perovskite layer to the solvent of 2D TMC dispersions. Importantly, the incorporation of 2D TMCs into the device structure through one or two spin coating steps always increases the PCE of the device. In addition, different 2D TMC interlayers result in the improvement of specific photovoltaic parameters, indicating different beneficial effects of the investigated materials. To compare the devices that have different 2D TMC interlayers and to eliminate any uncontrollable effect between various fabrication batches, Fig. 2 plots the percentage relative change of PCE and of the other photovoltaic parameters measured for the most performing 2D TMC-incorporating PSCs compared to reference (without 2D TMCs) devices. Cells incorporating InSe and SnS_2 nanosheets exhibit a similar behavior, characterized by a substantial increase in their FF by 2.32% and 2.83%, respectively, along with a slight improvement in J_{sc}, and no change in V_{oc}, compared to the reference device. Differently, the device containing $MoSe_2$ nanosheets exhibits a decrease in FF by about 1.9% compared to the reference cell. Meanwhile the J_{sc} increases considerably by 2.95% and the V_{oc} increases by 1.42% compared to the reference cell. Notably, the devices incorporating SnS_2 nanosheets demonstrated the greatest relative PCE improvement of 5.05%, with a 2.83% increase in FF, resulting in a PCE as high as 18.5% and FF of 82%. Fig. S7† shows the external quantum efficiency spectrum of the best device.

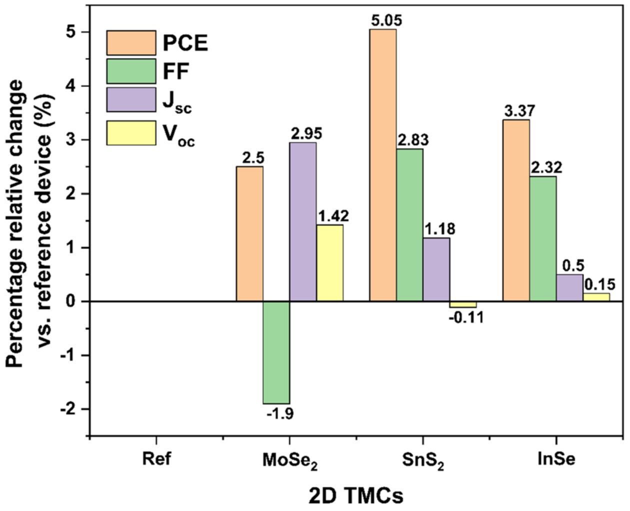

Fig. 2 Percentage relative change of PCE, FF, V_{oc}, and J_{sc} of 2D TMC-incorporating PSCs compared to reference (without 2D TMCs) PSCs.

The optoelectronic properties of the perovskite surface treated with 2D TMCs were investigated to assess if they are correlated with the device photovoltaic parameters. The W_F and valence band (VB) maximum energy of the perovskite surface were estimated using ambient photoemission spectroscopy measurements. Fig. S8† illustrates the W_F measurements of the perovskite surface before and after the deposition of 2D TMCs, and the extrapolated W_F values are listed in Table 1. The W_F of the pristine perovskite was determined to be 4.15 eV and increased after depositing the 2D TMCs (*i.e.*, 4.8 eV after SnS_2 nanosheet deposition). This behavior suggests the presence of a surface dipole that shifts the perovskite vacuum level to higher energies, with the negative part of the dipole facing outward from the surface (positive part facing toward the perovskite). The value of the interface dipole, $\varDelta$, for each case is listed in Table 1. Fig. S9† shows the VB measurements for the investigated samples. Interestingly, compared to the untreated

Table 1 Energy level values of the perovskite without 2D TMCs (reference) and the with 2D TMC interlayers at the perovskite/$PC_{70}BM$ interface. The CBO and VBO values are defined in the text and are calculated from eqn (1) and (2). $\varDelta$ is the size of the interface dipole at the perovskite interface

Perovskite	W_F (eV)	$\varDelta$ (eV)	VB (eV)	CB (eV)	CBO (eV)	VBO (eV)
Reference	−4.15		−5.41	−3.82	−0.08	−0.01
InSe	−4.46	0.31	−5.49	−3.9	0.00	−0.09
SnS2	−4.82	0.67	−5.47	−3.88	−0.02	−0.07
MoSe2	−4.73	0.58	−5.52	−3.93	0.03	−0.12

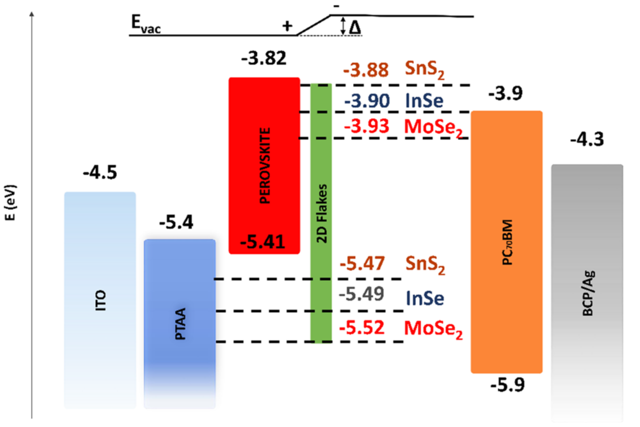

Fig. 3 Sketch of the energy level diagram of the investigated devices (energy values are not in scale). The dashed lines show the energy levels of the perovskite after the deposition of InSe, SnS_2, and $MoSe_2$ nanosheets.

perovskite, the presence of 2D TMCs shifts the perovskite VB to lower energy. Fig. 3 reports the sketch of the energy level diagram expected for the investigated cell configurations. The incorporation of 2D TMCs alters the energy level alignment at the interfaces between the perovskite and the $PC_{70}BM$. Specifically, the conduction band (CB) minimum energy and VB maximum energy shift to lower values. Thus, the CB minimum energy of the perovskite approaches that of $PC_{70}BM$, while the VB maximum energy of the perovskite moves away from that of PTAA. To quantify the offset of the energy levels, the energy difference between the CB minimum energies (conduction band offset-CBO) and the difference between the VB maximum energies (valence band offset-VBO) of the respective charge transporting layers and the perovskite were evaluated. In greater detail, the CBO and VBO can be calculated as:

$$\mathrm{CBO} = \chi_{\mathrm{perovskite}} - \chi_{\mathrm{PCBM}} \quad (1)$$

$$\mathrm{VBO} = \chi_{\mathrm{PTAA}} + E_{\mathrm{g,PTAA}} - (\chi_{\mathrm{perovskite}} + E_{\mathrm{g,perovskite}}) \quad (2)$$

in which χ is the electron affinity and E_g is the bandgap of the material indicated in the subscript.

The measured values for VB maximum energies and the calculated values for CBO and VBO are listed in Table 1. For the reference device, the CBO is negative (−0.08 eV), indicating that the CB minimum energy of $PC_{70}BM$ is lower than that of the perovskite. This energy level alignment at the perovskite/$PC_{70}BM$ interface is commonly indicated as a "cliff," signifying the absence of an energy barrier for electron injection from the perovskite to the $PC_{70}BM$. Similarly, the VBO for the reference device is −0.01 eV, implying no injection barrier for holes at the PTAA/perovskite interface. However, the CBO and VBO change drastically upon the deposition of 2D TMCs atop the perovskite. The CBO is reduced to −0.02 eV after the deposition of SnS_2 nanosheets and becomes 0.00 eV after depositing InSe nanosheets. Conversely, the CBO is positive (0.03 eV) when $MoSe_2$ nanosheets are deposited atop the perovskite, resulting in the formation of a "spike" feature at the perovskite/$PC_{70}BM$ interface.

In our previous work, we have demonstrated that the doping of the perovskite with BiTeI nanosheets leads to a modification of the energy levels of the perovskite.[88] In this context, increasing the CBO and decreasing the VBO have proven to be advantageous for device performance. Similar to our previous findings, tuning the CBO and VBO by incorporating TMC interlayers enhances the FF and, thus, the PCE of PSCs, as demonstrated for PSCs containing InSe and SnS_2 nanosheets. In the case of $MoSe_2$-containing PSCs, the formation of a "spike" level alignment at the interface is also expected to enhance the FF. However, a decrease in FF was observed together with an increase in V_{oc}, suggesting a different behavior of $MoSe_2$ nanosheets compared to SnS_2 and InSe nanosheets. The VBO of the reference sample (−0.01 eV) decreases to −0.12 eV with the incorporation of the $MoSe_2$ interlayer. Our previous work has demonstrated that lowering the VBO is advantageous for device performance, as it reduces non-radiative recombination at the interface between the HTL (PTAA) and the perovskite.[88] Moreover, experimental and theoretical studies have emphasized the importance of an absolute energy level offset of approximately 0.2 eV at the PTAA/perovskite interface.[89] Additionally, a VBO between 0 and −0.18 eV has been identified as the optimum range for efficient hole extraction.[90] Therefore, the observed improvement in V_{oc} for $MoSe_2$ can be attributed to the reduced recombination at the PTAA/perovskite interface, as the incorporation of $MoSe_2$ helps to tune the VBO closer to the theoretically optimum range. The improved PCE of devices incorporating InSe can be attributed to the tendency of this material to oxidize under ambient conditions, forming In_2O_3. Notably, the surface of InSe readily undergoes oxidation when subjected to air heat treatment.[91–93] The native oxide In_2O_3 is an n-type semiconductor with an optical band gap of 3.66 eV[92] and a high carrier concentration of approximately 6×10^{19} cm^{-3},[68,94] which can improve device PCE. Theoretical studies have indicated that H_2O, N_2, and O_2 molecules physisorbed onto the 2D InSe surface, resulting in partial electron charge transfer from InSe to the adsorbed molecules.[95] Additionally, it has been shown that a monolayer of InSe readily physisorbs H_2O under ambient conditions, irrespective of the presence of In or Se vacancies. Depending on the vacancies, InSe can be doped with H_2O, leading to either p-type (In vacancies) or n-type (Se vacancies) behavior,[96] suggesting precaution to assess the actual role of the InSe interlayers. The interface dipole at the interface of perovskite/ETL could reduce interface recombination, by preventing electron carriers in the ETL from reaching the interface.

The incorporation of 2D TMCs atop the perovskite has been the subject of extensive research, and our findings supplement previous studies, mainly focused on dichalcogenides and normal PSCs. Indeed, we have observed a strong agreement between our results and a theoretical study investigating the perovskite/InSe interface,[97] in which it was shown that InSe plays a crucial role in facilitating electron charge transport, causing charge transfer from the perovskite towards the InSe. In line with this, we have observed that the W_F of the perovskite surface covered with InSe nanosheets is higher than that of the control sample, indicating the accumulation of negative charge on the top surface with InSe, forming an interface dipole, as well as for the other investigated 2D TMCs.[97] Furthermore, experimental evidence has shown that the interfaces of TMCs such as MoS_2, WSe_2, and $MoSe_2$ with inorganic perovskites exhibit ultrafast and efficient charge carrier transfer.[98,99] Based on these findings, it is expected that the presence of 2D TMCs on the perovskite will not impede charge transport, a hypothesis that is confirmed by our experimental results. Moreover, SnS_2 nanosheets have been utilized in the literature to form the ETL, enhancing charge extraction and passivating interfacial traps more efficiently compared to SnO_2.[38] Our results are aligned with this, further supporting the beneficial effects of SnS_2 as an ETL in PSCs. Consequently, our study provides additional insights on the incorporation of the 2D TMC interlayer at the perovskite/$PC_{70}BM$ interface, highlighting their potential in improving charge extraction in PSCs.

Lifetime measurements

The stability of the PSCs incorporating TMC nanosheets was investigated following the International Summit on Organic Photovoltaic Stability (ISOS) L-2 protocol. Thus, the devices were subjected to continuous 1 sun illumination under ambient humidity at 65 °C.[100] Fig. 4 illustrates the normalized PCE of the unencapsulated devices over time. The reference device exhibited a burn-in phase during the initial testing period and a fast degradation afterwards. This behavior can be attributed to the degradation of the Ag electrode caused by its reaction with iodine, which migrated from the perovskite layer.[101–103] The device incorporating SnS_2 nanosheets showed the worst stability, while the one containing $MoSe_2$ nanosheets exhibited similar behavior to the reference cell. On the other hand, the incorporation of InSe led to the disappearance of the burn-in phase, enhancing the cell stability. The InSe-incorporating PSC exhibited a T_{70} of 250 h, *i.e.*, the device retained 70% of its initial PCE after 250 h. The superior stability of the InSe-containing PSC compared to the other cells can be correlated with the morphological and chemical properties of InSe nanosheets. The photo-induced degradation of InSe towards In_2Se_3 and In_2O_3 under ambient conditions can commence a surface passivation interlayer at the perovskite/ETL interface. The formation of In_2Se_3 and In_2O_3 (ref. 104) does not seem to affect the PCE and enhances the stability of the device, according to our results. Moreover, the InSe nanosheets show the highest lateral size amongst the investigated flakes (Fig. S1†) and therefore, InSe can serve as an effective barrier, protecting the metal electrode from the degradation species of the perovskite, thus enhancing the device stability.

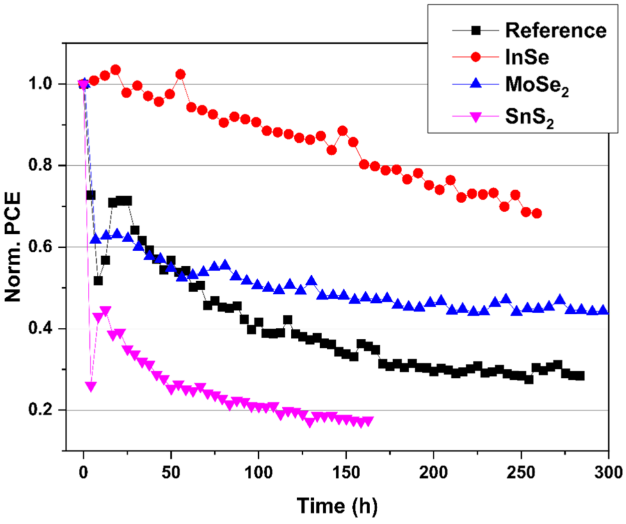

Fig. 4 Stability measurements of the PSCs incorporating InSe, $MoSe_2$, and SnS_2 interlayers under continuous 1 sun illumination, ambient humidity and 65 °C temperature (ISOS L-2).

Conclusions

The structure of inverted PSCs has been systematically optimized by screening the incorporation of various 2D TMCs in the form of an interlayer between the perovskite and the $PC_{70}BM$ ETL. Specifically, bulk InSe, SnS_2, and $MoSe_2$ were exfoliated by means of ultrasonication-assisted LPE and deposited atop the perovskite surface by spin coating to form thin (nanometer-thick) films. The incorporation of TMC interlayers causes a shift in the energy levels towards lower energies, altering the energy level offset at perovskite/charge-transporting layer interfaces. In detail, the introduction of SnS_2 and InSe nanosheets reduces the energy offset at the perovskite/$PC_{70}BM$ interface, resulting in an increase of the FF and PCE of the devices. The SnS_2- and InSe-incorporating devices exhibited relative improvement in PCE by 5.05% and 3.37%, respectively, compared to reference (without 2D TMCs) cells. The PSCs engineered with the SnS_2 interlayer showed the highest PCE, reaching 18.5% and FF of 82%. Conversely, the $MoSe_2$ interlayer introduces a small cliff arrangement at the interface of perovskite/$PC_{70}BM$. Compared to reference cells, the cells of $MoSe_2$-incorporating devices demonstrated improved PCE compared to reference cells, increasing the J_{sc} and V_{oc}. Moreover, to assess the long-term stability of the cells, the devices were subjected to continuous 1 sun illumination at 65 °C, following the ISOS-L2 ageing protocol. The results indicate different stability behaviors of the cells incorporating the investigated TMC interlayers, reflecting the different physico-chemical properties of the 2D TMCs. The incorporation of the $MoSe_2$ interlayer has no discernible effect on device stability, while the SnS_2 interlayer has a negative impact. On the other hand, InSe interlayer eliminates the burn-in degradation observed in the reference devices, significantly improving the overall cell stability. In summary, this work elucidates the potential of 2D TMCs to engineer the architecture of inverted PSCs.

Conflicts of interest

There are no conflicts of interest to declare.

Acknowledgements

We thank the Microelectronic Research Group at the University of Crete and Aleka Manousaki for the SEM images of the perovskite films, and Dr Manolis Spanakis from the Materials Science and Technology Department of the University of Crete, for the XPS measurements. The work has been supported by the European Union's Horizon Europe Framework Programme for research and innovation under grant agreement no. 694101—2D-PRINTABLE and by the European Union's Horizon 2020 research and innovation program under the Project EMERGE. The EMERGE project has received funding under grant agreement no. 101008701. Z. S. was supported by the ERC-CZ program (project LL2101) from the Ministry of Education Youth and Sports (MEYS) and used large infrastructure from project reg. no. CZ.02.1.01/0.0/0.0/15_003/0000444 financed by the EFRR.

References

1 S. Bellani, F. Wang, G. Longoni, L. Najafi, R. Oropesa-Nuñez, A. E. D. R. Castillo, M. Prato, X. Zhuang, V. Pellegrini, X. Feng and F. Bonaccorso, WS_2–Graphite Dual-Ion Batteries, *Nano Lett.*, 2018, **18**(11), 7155–7164.

2 H. Beydaghi, S. Bellani, L. Najafi, R. Oropesa-Nuñez, G. Bianca, A. Bagheri, I. Conticello, B. Martín-García, S. Kashefi, M. Serri, L. Liao, Z. Sofer, V. Pellegrini and F. Bonaccorso, Sulfonated NbS_2-based proton-exchange membranes for vanadium redox flow batteries, *Nanoscale*, 2022, **14**(16), 6152–6161.

3 A. Bagheri, S. Bellani, H. Beydaghi, M. Eredia, L. Najafi, G. Bianca, M. I. Zappia, M. Safarpour, M. Najafi, E. Mantero, Z. Sofer, G. Hou, V. Pellegrini, X. Feng and F. Bonaccorso, Functionalized Metallic 2D Transition Metal Dichalcogenide-Based Solid-State Electrolyte for Flexible All-Solid-State Supercapacitors, *ACS Nano*, 2022, **16**(10), 16426–16442.

4 L. Najafi, S. Bellani, R. Oropesa-Nuñez, B. Martín-García, M. Prato, L. Pasquale, J.-K. Panda, P. Marvan, Z. Sofer and F. Bonaccorso, TaS_2, $TaSe_2$, and Their Heterogeneous Films as Catalysts for the Hydrogen Evolution Reaction, *ACS Catal.*, 2020, **10**(5), 3313–3325.

5 L. Najafi, S. Bellani, R. Oropesa-Nuñez, R. Brescia, M. Prato, L. Pasquale, C. Demirci, F. Drago, B. Martín-García, J. Luxa, L. Manna, Z. Sofer and F. Bonaccorso, Microwave-Induced Structural Engineering and Pt Trapping in 6R-TaS_2 for the Hydrogen Evolution Reaction, *Small*, 2020, **16**(50), 2003372.

6 L. Najafi, R. Oropesa-Nuñez, S. Bellani, B. Martín-García, L. Pasquale, M. Serri, F. Drago, J. Luxa, Z. Sofer, D. Sedmidubský, R. Brescia, S. Lauciello, M. I. Zappia, D. V. Shinde, L. Manna and F. Bonaccorso, Topochemical Transformation of Two-Dimensional VSe_2 into Metallic Nonlayered VO_2 for Water Splitting Reactions in Acidic and Alkaline Media, *ACS Nano*, 2022, **16**(1), 351–367.

7 L. Najafi, S. Bellani, M. I. Zappia, M. Serri, R. Oropesa-Nuñez, A. Bagheri, H. Beydaghi, R. Brescia, L. Pasquale, D. V. Shinde, Y. Zuo, F. Drago, K. Mosina, Z. Sofer, L. Manna and F. Bonaccorso, Transition metal dichalcogenides as catalysts for the hydrogen evolution reaction: the emblematic case of 'inert' $ZrSe_2$ as catalyst for electrolyzers, *Nano Sel.*, 2022, **3**(6), 1069–1081.

8 E. D. Koutsouroubi, I. Vamvasakis, M. G. Minotaki, I. T. Papadas, C. Drivas, S. A. Choulis, G. Kopidakis, S. Kennou and G. S. Armatas, Ni-doped MoS_2 modified graphitic carbon nitride layered hetero-nanostructures as highly efficient photocatalysts for environmental remediation, *Appl. Catal., B*, 2021, **297**, 120419.

9 S. Bellani, L. Najafi, A. Capasso, A. E. D. R. Castillo, M. R. Antognazza and F. Bonaccorso, Few-layer MoS_2 flakes as a hole-selective layer for solution-processed hybrid organic hydrogen-evolving photocathodes, *J. Mater. Chem. A*, 2017, **5**(9), 4384–4396.

10 L. Najafi, V. Romano, R. Oropesa-Nuñez, M. Prato, S. Lauciello, G. D'Angelo, S. Bellani and F. Bonaccorso, Hybrid Organic/Inorganic Photocathodes Based on WS_2 Flakes as Hole Transporting Layer Material, *Small Struct.*, 2021, **2**(3), 2000098.

11 D. N. Kouvatsos, G. Papadimitropoulos, T. Spiliotis, M. Vasilopoulou, D. Barreca, A. Gasparotto and D. Davazoglou, Electrical characteristics of vapor deposited amorphous MoS_2 two-terminal structures and back gate thin film transistors with Al, Au, Cu and Ni-Au contacts, *Phys. Status Solidi C*, 2015, **12**(7), 975–979.

12 K. F. Mak and J. Shan, Photonics and optoelectronics of 2D semiconductor transition metal dichalcogenides, *Nat. Photonics*, 2016, **10**(4), 216–226.

13 M. I. Zappia, G. Bianca, S. Bellani, M. Serri, L. Najafi, R. Oropesa-Nuñez, B. Martín-García, D. Bouša, D. Sedmidubský, V. Pellegrini, Z. Sofer, A. Cupolillo and F. Bonaccorso, Solution-Processed GaSe Nanoflake-Based Films for Photoelectrochemical Water Splitting and Photoelectrochemical-Type Photodetectors, *Adv. Funct. Mater.*, 2020, **30**(10), 1909572.

14 I. Kriegel, M. Ghini, S. Bellani, K. Zhang, A. W. Jansons, B. M. Crockett, K. M. Koskela, E. S. Barnard, E. Penzo, J. E. Hutchison, J. A. Robinson, L. Manna, N. J. Borys and P. J. Schuck, Light-Driven Permanent Charge Separation across a Hybrid Zero-Dimensional/Two-Dimensional Interface, *J. Phys. Chem. C*, 2020, **124**(14), 8000–8007.

15 G. Bianca, M. I. Zappia, S. Bellani, Z. Sofer, M. Serri, L. Najafi, R. Oropesa-Nuñez, B. Martín-García, T. Hartman, L. Leoncino, D. Sedmidubský, V. Pellegrini, G. Chiarello and F. Bonaccorso, Liquid-Phase Exfoliated GeSe Nanoflakes for Photoelectrochemical-Type Photodetectors and Photoelectrochemical Water Splitting, *ACS Appl. Mater. Interfaces*, **2020**, 48598–48613.

16 M. I. Zappia, G. Bianca, S. Bellani, N. Curreli, Z. Sofer, M. Serri, L. Najafi, M. Piccinni, R. Oropesa-Nuñez, P. Marvan, V. Pellegrini, I. Kriegel, M. Prato, A. Cupolillo and F. Bonaccorso, Two-Dimensional Gallium Sulfide Nanoflakes for UV-Selective Photoelectrochemical-type Photodetectors, *J. Phys. Chem. C*, 2021, **125**(22), 11857–11866.

17 G. Bianca, M. I. Zappia, S. Bellani, M. Ghini, N. Curreli, J. Buha, V. Galli, M. Prato, A. Soll, Z. Sofer, G. Lanzani, I. Kriegel and F. Bonaccorso, Indium Selenide/Indium Tin Oxide Hybrid Films for Solution-Processed

Photoelectrochemical-Type Photodetectors in Aqueous Media, *Adv. Mater. Interfaces*, 2023, **10**(1), 2201635.

18 K. N. Nazif, A. Daus, J. Hong, N. Lee, S. Vaziri, A. Kumar, F. Nitta, M. E. Chen, S. Kananian, R. Islam, K.-H. Kim, J.-H. Park, A. S. Y. Poon, M. L. Brongersma, E. Pop and K. C. Saraswat, High-specific-power flexible transition metal dichalcogenide solar cells, *Nat. Commun.*, 2021, **12**(1), 7034.

19 S. Aftab, M. Z. Iqbal, S. Hussain, H. H. Hegazy and M. A. Saeed, Transition metal dichalcogenides solar cells and integration with perovskites, *Nano Energy*, 2023, **108**, 108249.

20 S. Das, D. Pandey, J. Thomas and T. Roy, The Role of Graphene and Other 2D Materials in Solar Photovoltaics, *Adv. Mater.*, 2019, **31**(1), 1802722.

21 T. He, C. Lan, S. Zhou, Y. Li, Y. Yin, C. Li and Y. Liu, Enhanced responsivity of a graphene/Si-based heterostructure broadband photodetector by introducing a WS_2 interfacial layer, *J. Mater. Chem. C*, 2021, **9**(11), 3846–3853.

22 Y. Tsuboi, F. Wang, D. Kozawa, K. Funahashi, S. Mouri, Y. Miyauchi, T. Takenobu and K. Matsuda, Enhanced photovoltaic performances of graphene/Si solar cells by insertion of a MoS_2 thin film, *Nanoscale*, 2015, **7**(34), 14476–14482.

23 G. Kakavelakis, A. E. Del Rio Castillo, V. Pellegrini, A. Ansaldo, P. Tzourmpakis, R. Brescia, M. Prato, E. Stratakis, E. Kymakis and F. Bonaccorso, Size-Tuning of WSe_2 Flakes for High Efficiency Inverted Organic Solar Cells, *ACS Nano*, 2017, **11**(4), 3517–3531.

24 S. Bellani, A. Bartolotta, A. Agresti, G. Calogero, G. Grancini, A. Di Carlo, E. Kymakis and F. Bonaccorso, Solution-processed two-dimensional materials for next-generation photovoltaics, *Chem. Soc. Rev.*, 2021, **50**(21), 11870–11965.

25 L. C. Palilis, M. Vasilopoulou, A. Verykios, A. Soultati, E. Polydorou, P. Argitis, D. Davazoglou, A. R. b. M. Yusoff and M. K. Nazeeruddin, Inorganic and Hybrid Interfacial Materials for Organic and Perovskite Solar Cells, *Adv. Energy Mater.*, 2020, **10**(27), 2000910.

26 D. Tsikritzis, K. Rogdakis, K. Chatzimanolis, M. Petrović, N. Tzoganakis, L. Najafi, B. Martín-García, R. Oropesa-Nuñez, S. Bellani, A. E. D. R. Castillo, M. Prato, M. M. Stylianakis, F. Bonaccorso and E. Kymakis, A two-fold engineering approach based on Bi_2Te_3 flakes towards efficient and stable inverted perovskite solar cells, *Mater. Adv.*, 2020, **1**(3), 450–462.

27 N. H. Hemasiri, S. Kazim and S. Ahmad, Reduced trap density and mitigating the interfacial losses by placing 2D dichalcogenide material at perovskite/HTM interface in a dopant free perovskite solar cells, *Nano Energy*, 2020, **77**, 105292.

28 A. Capasso, F. Matteocci, L. Najafi, M. Prato, J. Buha, L. Cinà, V. Pellegrini, A. D. Carlo and F. Bonaccorso, Few-Layer MoS_2 Flakes as Active Buffer Layer for Stable Perovskite Solar Cells, *Adv. Energy Mater.*, 2016, **6**(16), 1600920.

29 L. Najafi, B. Taheri, B. Martín-García, S. Bellani, D. Di Girolamo, A. Agresti, R. Oropesa-Nuñez, S. Pescetelli, L. Vesce, E. Calabrò, M. Prato, A. E. D. R. Castillo, A. D. Carlo and F. Bonaccorso, MoS_2 Quantum Dot/Graphene Hybrids for Advanced Interface Engineering of a $CH_3NH_3PbI_3$ Perovskite Solar Cell with an Efficiency of over 20%, *ACS Nano*, 2018, **12**(11), 10736–10754.

30 M. Liang, A. Ali, A. Belaidi, M. I. Hossain, O. Ronan, C. Downing, N. Tabet, S. Sanvito, F. EI-Mellouhi and V. Nicolosi, Improving stability of organometallic-halide perovskite solar cells using exfoliation two-dimensional molybdenum chalcogenides, *npj 2D Mater. Appl.*, 2020, **4**(1), 40.

31 Y. Busby, A. Agresti, S. Pescetelli, A. Di Carlo, C. Noel, J.-J. Pireaux and L. Houssiau, Aging effects in interface-engineered perovskite solar cells with 2D nanomaterials: a depth profile analysis, *Mater. Today Energy*, 2018, **9**, 1–10.

32 G. Tang, P. You, Q. Tai, A. Yang, J. Cao, F. Zheng, Z. Zhou, J. Zhao, P. K. L. Chan and F. Yan, Solution-Phase Epitaxial Growth of Perovskite Films on 2D Material Flakes for High-Performance Solar Cells, *Adv. Mater.*, 2019, **31**(24), 1807689.

33 A. Agresti, S. Pescetelli, A. L. Palma, B. Martín-García, L. Najafi, S. Bellani, I. Moreels, M. Prato, F. Bonaccorso and A. Di Carlo, Two-Dimensional Material Interface Engineering for Efficient Perovskite Large-Area Modules, *ACS Energy Lett.*, 2019, **4**(8), 1862–1871.

34 S. Pescetelli, A. Agresti, S. Razza, H. Pazniak, L. Najafi, F. Bonaccorso and A. D. Carlo, Synergic use of two-dimensional materials to tailor interfaces in large area perovskite modules, *Nano Energy*, 2022, **95**, 107019.

35 P. You, G. Tang and F. Yan, Two-dimensional materials in perovskite solar cells, *Mater. Today Energy*, 2019, **11**, 128–158.

36 Y. G. Kim, K. C. Kwon, Q. V. Le, K. Hong, H. W. Jang and S. Y. Kim, Atomically thin two-dimensional materials as hole extraction layers in organolead halide perovskite photovoltaic cells, *J. Power Sources*, 2016, **319**, 1–8.

37 B. Peng, G. Yu, Y. Zhao, Q. Xu, G. Xing, X. Liu, D. Fu, B. Liu, J. R. S. Tan, W. Tang, H. Lu, J. Xie, L. Deng, T. C. Sum and K. P. Loh, Achieving Ultrafast Hole Transfer at the Monolayer MoS_2 and $CH_3NH_3PbI_3$ Perovskite Interface by Defect Engineering, *ACS Nano*, 2016, **10**(6), 6383–6391.

38 X. Zhao, S. Liu, H. Zhang, S.-Y. Chang, W. Huang, B. Zhu, Y. Shen, C. Shen, D. Wang, Y. Yang and M. Wang, 20% Efficient Perovskite Solar Cells with 2D Electron Transporting Layer, *Adv. Funct. Mater.*, 2019, **29**(4), 1805168.

39 L.-C. Chen, Z.-L. Tseng, C.-C. Chen, S. H. Chang and C.-H. Ho, Fabrication and characteristics of $CH_3NH_3PbI_3$ perovskite solar cells with molybdenum-selenide hole-transport layer, *Appl. Phys. Express*, 2016, **9**(12), 122301.

40 Y. Choi, S. Jung, N. K. Oh, J. Lee, J. Seo, U. Kim, D. Koo and H. Park, Enhanced Charge Transport via Metallic 1T Phase Transition Metal Dichalcogenides-Mediated Hole Transport Layer Engineering for Perovskite Solar Cells, *ChemNanoMat*, 2019, **5**(8), 1050–1058.

41 D. Wang, N. K. Elumalai, M. A. Mahmud, H. Yi, M. B. Upama, R. A. L. Chin, G. Conibeer, C. Xu, F. Haque, L. Duan and A. Uddin, MoS_2 incorporated hybrid hole transport layer for high performance and stable perovskite solar cells, *Synth. Met.*, 2018, **246**, 195–203.

42 R. Dai, Y. Wang, J. Wang and X. Deng, Metal–Organic-Compound-Modified MoS_2 with Enhanced Solubility for High-Performance Perovskite Solar Cells, *ChemSusChem*, 2017, **10**(14), 2869–2874.

43 M. Imran, H. Coşkun, F. H. Isikgor, L. Bichen, N. A. Khan and J. Ouyang, Highly efficient and stable inverted perovskite solar cells with two-dimensional ZnSe deposited using a thermal evaporator for electron collection, *J. Mater. Chem. A*, 2018, **6**(45), 22713–22720.

44 Y. Wang, S. Wang, X. Chen, Z. Li, J. Wang, T. Li and X. Deng, Largely enhanced V_{OC} and stability in perovskite solar cells with modified energy match by coupled 2D interlayers, *J. Mater. Chem. A*, 2018, **6**(11), 4860–4867.

45 K. Chatzimanolis, K. Rogdakis, D. Tsikritzis, N. Tzoganakis, M. Tountas, M. Krassas, S. Bellani, L. Najafi, B. Martín-García, R. Oropesa-Nuñez, M. Prato, G. Bianca, I. Plutnarova, Z. Sofer, F. Bonaccorso and E. Kymakis, Inverted perovskite solar cells with enhanced lifetime and thermal stability enabled by a metallic tantalum disulfide buffer layer, *Nanoscale Adv.*, 2021, **3**(11), 3124–3135.

46 S. Pescetelli, A. Agresti, G. Viskadouros, S. Razza, K. Rogdakis, I. Kalogerakis, E. Spiliarotis, E. Leonardi, P. Mariani, L. Sorbello, M. Pierro, C. Cornaro, S. Bellani, L. Najafi, B. Martín-García, A. E. D. R. Castillo, R. Oropesa-Nuñez, M. Prato, S. Maranghi, M. L. Parisi, A. Sinicropi, R. Basosi, F. Bonaccorso, E. Kymakis and A. D. Carlo, Integration of two-dimensional materials-based perovskite solar panels into a stand-alone solar farm, *Nat. Energy*, 2022, **7**(7), 597–607.

47 B. A. Parkinson, Dye sensitization of van der Waals surfaces of tin disulfide photoanodes, *Langmuir*, 1988, **4**(4), 967–976.

48 Y. Sun, H. Cheng, S. Gao, Z. Sun, Q. Liu, Q. Liu, F. Lei, T. Yao, J. He, S. Wei and Y. Xie, Freestanding Tin Disulfide Single-Layers Realizing Efficient Visible-Light Water Splitting, *Angew. Chem., Int. Ed.*, 2012, **51**(35), 8727–8731.

49 D. De, J. Manongdo, S. See, V. Zhang, A. Guloy and H. Peng, High on/off ratio field effect transistors based on exfoliated crystalline SnS_2 nano-membranes, *Nanotechnology*, 2013, **24**(2), 025202.

50 Y. Huang, E. Sutter, J. T. Sadowski, M. Cotlet, O. L. A. Monti, D. A. Racke, M. R. Neupane, D. Wickramaratne, R. K. Lake, B. A. Parkinson and P. Sutter, Tin disulfide-an emerging layered metal dichalcogenide semiconductor: materials properties and device characteristics, *ACS Nano*, 2014, **8**(10), 10743–10755.

51 P. Patil, D. S. Mann, U. T. Nakate, Y.-B. Hahn, S.-N. Kwon and S.-I. Na, Hybrid interfacial ETL engineering using PCBM-SnS_2 for High-Performance p-i-n structured planar perovskite solar cells, *Chem. Eng. J.*, 2020, **397**, 125504.

52 E. Zhao, L. Gao, S. Yang, L. Wang, J. Cao and T. Ma, In situ fabrication of 2D SnS_2 nanosheets as a new electron transport layer for perovskite solar cells, *Nano Res.*, 2018, **11**(11), 5913–5923.

53 Y. Zhang, T.-R. Chang, B. Zhou, Y.-T. Cui, H. Yan, Z. Liu, F. Schmitt, J. Lee, R. Moore, Y. Chen, H. Lin, H.-T. Jeng, S.-K. Mo, Z. Hussain, A. Bansil and Z.-X. Shen, Direct observation of the transition from indirect to direct bandgap in atomically thin epitaxial $MoSe_2$, *Nat. Nanotechnol.*, 2014, **9**(2), 111–115.

54 P. Tonndorf, R. Schmidt, P. Böttger, X. Zhang, J. Börner, A. Liebig, M. Albrecht, C. Kloc, O. Gordan, D. R. T. Zahn, S. M. d. Vasconcellos and R. Bratschitsch, Photoluminescence emission and Raman response of monolayer MoS_2, $MoSe_2$, and WSe_2, *Opt. Express*, 2013, **21**(4), 4908.

55 N. R. Pradhan, D. Rhodes, Y. Xin, S. Memaran, L. Bhaskaran, M. Siddiq, S. Hill, P. M. Ajayan and L. Balicas, Ambipolar Molybdenum Diselenide Field-Effect Transistors: Field-Effect and Hall Mobilities, *ACS Nano*, 2014, **8**(8), 7923–7929.

56 L.-B. Chang, C.-C. Tseng, J.-H. Lee, G.-M. Wu, M.-J. Jeng, W.-S. Feng, D. W. Chen, L.-C. Chen, K.-L. Lee, E. Popko, L. Jacak and K. Gwozdz, Preparation and characterization of $MoSe_2/CH_3NH_3PbI_3$/PMMA perovskite solar cells using polyethylene glycol solution, *Vacuum*, 2020, **178**, 109441.

57 A. Jäger-Waldau, M. Ch. Lux-Steiner and E. Bucher, MoS_2, $MoSe_2$, WS_2 and WSe_2 Thin Films for Photovoltaics, *Solid State Phenom.*, 1994, **37–38**, 479–484.

58 L. Najafi, S. Bellani, R. Oropesa-Nuñez, A. Ansaldo, M. Prato, A. E. D. R. Castillo and F. Bonaccorso, Engineered $MoSe_2$ -Based Heterostructures for Efficient Electrochemical Hydrogen Evolution Reaction, *Adv. Energy Mater.*, 2018, **8**(16), 1703212.

59 L. Najafi, S. Bellani, R. Oropesa-Nuñez, M. Prato, B. Martín-García, R. Brescia and F. Bonaccorso, Carbon Nanotube-Supported $MoSe_2$ Holey Flake:Mo_2C Ball Hybrids for Bifunctional pH-Universal Water Splitting, *ACS Nano*, 2019, **13**(3), 3162–3176.

60 X. Liu, J.-Z. Zhang, K.-J. Huang and P. Hao, Net-like molybdenum selenide–acetylene black supported on Ni foam for high-performance supercapacitor electrodes and hydrogen evolution reaction, *Chem. Eng. J.*, 2016, **302**, 437–445.

61 X. Yang, Z. Zhang and X. Shi, Rational design of coaxial-cable $MoSe_2$/C: towards high performance electrode materials for lithium-ion and sodium-ion batteries, *J. Alloys Compd.*, 2016, **686**, 413–420.

62 N. Curreli, M. Serri, D. Spirito, E. Lago, E. Petroni, B. Martín-García, A. Politano, B. Gürbulak, S. Duman, R. Krahne, V. Pellegrini and F. Bonaccorso, Liquid Phase Exfoliated Indium Selenide Based Highly Sensitive Photodetectors, *Adv. Funct. Mater.*, 2020, **30**(13), 1908427.

63 G. Bianca, M. I. Zappia, S. Bellani, M. Ghini, N. Curreli, J. Buha, V. Galli, M. Prato, A. Soll, Z. Sofer, G. Lanzani, I. Kriegel and F. Bonaccorso, Indium Selenide/Indium Tin Oxide Hybrid Films for Solution-Processed Photoelectrochemical-Type Photodetectors in Aqueous Media, *Adv. Mater. Interfaces*, 2023, **10**(1), 2201635.

64 E. Petroni, E. Lago, S. Bellani, D. W. Boukhvalov, A. Politano, B. Gürbulak, S. Duman, M. Prato, S. Gentiluomo, R. Oropesa-Nuñez, J.-K. Panda, P. S. Toth, A. E. D. R. Castillo, V. Pellegrini and F. Bonaccorso, Liquid-Phase Exfoliated Indium-Selenide Flakes and Their Application in Hydrogen Evolution Reaction, *Small*, 2018, **14**(26), 1800749.

65 G. W. Mudd, S. A. Svatek, T. Ren, A. Patanè, O. Makarovsky, L. Eaves, P. H. Beton, Z. D. Kovalyuk, G. V. Lashkarev, Z. R. Kudrynskyi and A. I. Dmitriev, Tuning the Bandgap of Exfoliated InSe Nanosheets by Quantum Confinement, *Adv. Mater.*, 2013, **25**(40), 5714–5718.

66 S. Lei, L. Ge, S. Najmaei, A. George, R. Kappera, J. Lou, M. Chhowalla, H. Yamaguchi, G. Gupta, R. Vajtai, A. D. Mohite and P. M. Ajayan, Evolution of the Electronic Band Structure and Efficient Photo-Detection in Atomic Layers of InSe, *ACS Nano*, 2014, **8**(2), 1263–1272.

67 M. Brotons-Gisbert, D. Andres-Penares, J. Suh, F. Hidalgo, R. Abargues, P. J. Rodríguez-Cantó, A. Segura, A. Cros, G. Tobias, E. Canadell, P. Ordejón, J. Wu, J. P. Martínez-Pastor and J. F. Sánchez-Royo, Nanotexturing To Enhance Photoluminescent Response of Atomically Thin Indium Selenide with Highly Tunable Band Gap, *Nano Lett.*, 2016, **16**(5), 3221–3229.

68 O. Lang, C. Pettenkofer, J. F. Sánchez-Royo, A. Segura, A. Klein and W. Jaegermann, Thin film growth and band lineup of In_2O_3 on the layered semiconductor InSe, *J. Appl. Phys.*, 1999, **86**(10), 5687–5691.

69 D. A. Bandurin, A. V. Tyurnina, G. L. Yu, A. Mishchenko, V. Zólyomi, S. V. Morozov, R. K. Kumar, R. V. Gorbachev, Z. R. Kudrynskyi, S. Pezzini, Z. D. Kovalyuk, U. Zeitler, K. S. Novoselov, A. Patanè, L. Eaves, I. V. Grigorieva, V. I. Fal'ko, A. K. Geim and Y. Cao, High electron mobility, quantum Hall effect and anomalous optical response in atomically thin InSe, *Nat. Nanotechnol.*, 2017, **12**(3), 223–227.

70 S. Sucharitakul, N. J. Goble, U. R. Kumar, R. Sankar, Z. A. Bogorad, F.-C. Chou, Y.-T. Chen and X. P. A. Gao, Intrinsic Electron Mobility Exceeding 10^3 $cm^2/(V\ s)$ in Multilayer InSe FETs, *Nano Lett.*, 2015, **15**(6), 3815–3819.

71 W. Feng, W. Zheng, W. Cao and P. Hu, Back Gated Multilayer InSe Transistors with Enhanced Carrier Mobilities via the Suppression of Carrier Scattering from a Dielectric Interface, *Adv. Mater.*, 2014, **26**(38), 6587–6593.

72 J. Martínez-Pastor, A. Segura, J. L. Valdés and A. Chevy, Electrical and photovoltaic properties of indium-tin-oxide/p-InSe/Au solar cells, *J. Appl. Phys.*, 1987, **62**(4), 1477–1483.

73 J. F. Sánchez-Royo, A. Segura, O. Lang, C. Pettenkofer, W. Jaegermann, A. Chevy and L. Roa, Photovoltaic properties of indium selenide thin films prepared by van der Waals epitaxy, *Thin Solid Films*, 1997, **307**(1–2), 283–287.

74 J. Jiang, J. Li, Y. Li, J. Duan, L. Li, Y. Tian, Z. Zong, H. Zheng, X. Feng, Q. Li, H. Liu, Y. Zhang, T.-L. Ren and L. Han, Stable InSe transistors with high-field effect mobility for reliable nerve signal sensing, *npj 2D Mater. Appl.*, 2019, **3**(1), 29.

75 M. A. Airo, R. Rodrigues, S. Gqoba, N. Ntholeng, F. Otieno, M. J. Moloto, M. W. C. C. Greenshields, I. A. Hümmelgen and N. Moloto, Colloidal InSe nanostructures: effect of morphology on their chemical sensitivity to methanol and formaldehyde fumes, *Sens. Actuators, B*, 2016, **236**, 116–125.

76 N. T. Hung, A. R. T. Nugraha and R. Saito, Two-dimensional InSe as a potential thermoelectric material, *Appl. Phys. Lett.*, 2017, **111**(9), 092107.

77 K. Premasiri, S. K. Radha, S. Sucharitakul, U. R. Kumar, R. Sankar, F.-C. Chou, Y.-T. Chen and X. P. A. Gao, Tuning Rashba Spin–Orbit Coupling in Gated Multilayer InSe, *Nano Lett.*, 2018, **18**(7), 4403–4408.

78 C. Backes, A. M. Abdelkader, C. Alonso, A. Andrieux-Ledier, R. Arenal, J. Azpeitia, N. Balakrishnan, L. Banszerus, J. Barjon, R. Bartali, S. Bellani, C. Berger, R. Berger, M. M. B. Ortega, C. Bernard, P. H. Beton, A. Beyer, A. Bianco, P. Bøggild, F. Bonaccorso, G. B. Barin, C. Botas, R. A. Bueno, D. Carriazo, A. Castellanos-Gomez, M. Christian, A. Ciesielski, T. Ciuk, M. T. Cole, J. Coleman, C. Coletti, L. Crema, H. Cun, D. Dasler, D. De Fazio, N. Díez, S. Drieschner, G. S. Duesberg, R. Fasel, X. Feng, A. Fina, S. Forti, C. Galiotis, G. Garberoglio, J. M. García, J. A. Garrido, M. Gibertini, A. Gölzhäuser, J. Gómez, T. Greber, F. Hauke, A. Hemmi, I. Hernandez-Rodriguez, A. Hirsch, S. A. Hodge, Y. Huttel, P. U. Jepsen, I. Jimenez, U. Kaiser, T. Kaplas, H. Kim, A. Kis, K. Papagelis, K. Kostarelos, A. Krajewska, K. Lee, C. Li, H. Lipsanen, A. Liscio, M. R. Lohe, A. Loiseau, L. Lombardi, M. F. López, O. Martin, C. Martín, L. Martínez, J. A. Martin-Gago, J. I. Martínez, N. Marzari, Á. Mayoral, J. McManus, M. Melucci, J. Méndez, C. Merino, P. Merino, A. P. Meyer, E. Miniussi, V. Miseikis, N. Mishra, V. Morandi, C. Munuera, R. Muñoz, H. Nolan, L. Ortolani, A. K. Ott, I. Palacio, V. Palermo, J. Parthenios, I. Pasternak, A. Patane, M. Prato, H. Prevost, V. Prudkovskiy, N. Pugno, T. Rojo, A. Rossi, P. Ruffieux, P. Samorì, L. Schué, E. Setijadi, T. Seyller, G. Speranza, C. Stampfer, I. Stenger, W. Strupinski, Y. Svirko, S. Taioli, K. B. K. Teo, M. Testi, F. Tomarchio, M. Tortello, E. Treossi, A. Turchanin, E. Vazquez, E. Villaro, P. R. Whelan, Z. Xia, R. Yakimova, S. Yang, G. R. Yazdi, C. Yim, D. Yoon, X. Zhang, X. Zhuang, L. Colombo, A. C. Ferrari and M. Garcia-Hernandez, Production and processing of graphene and related materials, *2D Materials*, 2020, **7**(2), 022001.

79 L. Najafi, S. Bellani, R. Oropesa-Nuñez, A. Ansaldo, M. Prato, A. E. D. R. Castillo and F. Bonaccorso, Engineered MoSe2-Based Heterostructures for Efficient Electrochemical Hydrogen Evolution Reaction, *Adv. Energy Mater.*, 2018, **8**(16), 1703212.

80 L. Najafi, S. Bellani, R. Oropesa-Nuñez, A. Ansaldo, M. Prato, A. E. D. R. Castillo and F. Bonaccorso, Doped-$MoSe_2$ Nanoflakes/3d Metal Oxide–Hydr(Oxy)Oxides Hybrid Catalysts for pH-Universal Electrochemical Hydrogen Evolution Reaction, *Adv. Energy Mater.*, 2018, **8**(27), 1801764.

81 V. Zólyomi, N. D. Drummond and V. I. Fal'ko, Electrons and phonons in single layers of hexagonal indium

chalcogenides from ab initio calculations, *Phys. Rev. B: Condens. Matter Mater. Phys.*, 2014, **89**(20), 205416.

82 A. J. Smith, P. E. Meek and W. Y. Liang, Raman scattering studies of SnS_2 and $SnSe_2$, *J. Phys. C: Solid State Phys.*, 1977, **10**(8), 1321.

83 D. Nam, J.-U. Lee and H. Cheong, Excitation energy dependent Raman spectrum of $MoSe_2$, *Sci. Rep.*, 2015, **5**(1), 17113.

84 L. Najafi, S. Bellani, R. Oropesa-Nuñez, A. Ansaldo, M. Prato, A. E. D. R. Castillo and F. Bonaccorso, Engineered $MoSe_2$-Based Heterostructures for Efficient Electrochemical Hydrogen Evolution Reaction, *Adv. Energy Mater.*, 2018, **8**(16), 1703212.

85 S. K. A. Rahul and V. G. Sathe, Unraveling the phonon scattering mechanism in exfoliated $MoSe_2$ nanosheets using temperature-dependent Raman spectroscopy, *J. Mater. Sci.: Mater. Electron.*, 2022, **33**(31), 23964–23973.

86 T. Sriv, K. Kim and H. Cheong, Low-Frequency Raman Spectroscopy of Few-Layer 2H-SnS_2, *Sci. Rep.*, 2018, **8**(1), 10194.

87 N. Bhardwaj and S. Mohapatra, Fabrication Of SnO_2 Three Dimensional Complex Microcrystal Chains By Carbothermal Reduction Method, *Adv. Mater. Lett.*, 2015, **6**(2), 148–152.

88 D. Tsikritzis, K. Chatzimanolis, N. Tzoganakis, S. Bellani, M. I. Zappia, G. Bianca, N. Curreli, J. Buha, I. Kriegel, N. Antonatos, Z. Sofer, M. Krassas, K. Rogdakis, F. Bonaccorso and E. Kymakis, Two-dimensional BiTeI as a novel perovskite additive for printable perovskite solar cells, *Sustainable Energy Fuels*, 2022, **6**(23), 5345–5359.

89 A. A. B. Baloch, S. P. Aly, M. I. Hossain, F. El-Mellouhi, N. Tabet and F. H. Alharbi, Full space device optimization for solar cells, *Sci. Rep.*, 2017, **7**(1), 11984.

90 R. J. E. Westbrook, I. Sanchez-Molina, J. Manuel Marin-Beloqui, H. Bronstein and S. A. Haque, Effect of Interfacial Energetics on Charge Transfer from Lead Halide Perovskite to Organic Hole Conductors, *J. Phys. Chem. C*, 2018, **122**(2), 1326–1332.

91 N. Balakrishnan, Z. R. Kudrynskyi, E. F. Smith, M. W. Fay, O. Makarovsky, Z. D. Kovalyuk, L. Eaves, P. H. Beton and A. Patanè, Engineering p − n junctions and bandgap tuning of InSe nanolayers by controlled oxidation, *2D Materials*, 2017, **4**(2), 025043.

92 T. Siciliano, M. D. Giulio, M. Tepore, A. Genga, G. Micocci and A. Tepore, In_2O_3 films prepared by thermal oxidation of amorphous InSe thin films, *Thin Solid Films*, 2012, **520**(7), 2455–2460.

93 A. P. Bakhtinov, Z. D. Kovalyuk, O. N. Sydor, V. N. Katerinchuk and O. S. Lytvyn, Formation of nanostructure on the surface of layered InSe semiconductor caused by oxidation under heating, *Phys. Solid State*, 2007, **49**(8), 1572–1578.

94 J. E. Medvedeva, I. A. Zhuravlev, C. Burris, D. B. Buchholz, M. Grayson and R. P. H. Chang, Origin of high carrier concentration in amorphous wide-bandgap oxides: role of disorder in defect formation and electron localization in In_2O_{3-x}, *J. Appl. Phys.*, 2020, **127**(17), 175701.

95 D. Ma, W. Ju, Y. Tang and Y. Chen, First-principles study of the small molecule adsorption on the InSe monolayer, *Appl. Surf. Sci.*, 2017, **426**, 244–252.

96 D. Ma, T. Li, D. Yuan, C. He, Z. Lu, Z. Lu, Z. Yang and Y. Wang, The role of the intrinsic Se and In vacancies in the interaction of O_2 and H_2O molecules with the InSe monolayer, *Appl. Surf. Sci.*, 2018, **434**, 215–227.

97 S. K. Matta, C. Tang, A. P. O'Mullane, A. Du and S. P. Russo, Density Functional Theory Study of Two-Dimensional Post-Transition Metal Chalcogenides and Halides for Interfacial Charge Transport in Perovskite Solar Cells, *ACS Appl. Nano Mater.*, 2022, **5**(10), 14456–14463.

98 Q. Fang, Q. Shang, L. Zhao, R. Wang, Z. Zhang, P. Yang, X. Sui, X. Qiu, X. Liu, Q. Zhang and Y. Zhang, Ultrafast Charge Transfer in Perovskite Nanowire/2D Transition Metal Dichalcogenide Heterostructures, *J. Phys. Chem. Lett.*, 2018, **9**(7), 1655–1662.

99 A. Asaithambi, N. K. Tofighi, N. Curreli, M. De Franco, A. Patra, N. Petrini, D. Baranov, L. Manna, F. D. Stasio and I. Kriegel, Generation of Free Carriers in $MoSe_2$ Monolayers Via Energy Transfer from CsPbBr3 Nanocrystals, *Adv. Opt. Mater.*, 2022, **10**(14), 2200638.

100 M. V. Khenkin, E. A. Katz, A. Abate, G. Bardizza, J. J. Berry, C. Brabec, F. Brunetti, V. Bulović, Q. Burlingame, A. D. Carlo, R. Cheacharoen, Y.-B. Cheng, A. Colsmann, S. Cros, K. Domanski, M. Dusza, C. J. Fell, S. R. Forrest, Y. Galagan, D. D. Girolamo, M. Grätzel, A. Hagfeldt, E. von Hauff, H. Hoppe, J. Kettle, H. Köbler, M. S. Leite, S. Liu, Y.-L. Loo, J. M. Luther, C.-Q. Ma, M. Madsen, M. Manceau, M. Matheron, M. McGehee, R. Meitzner, M. K. Nazeeruddin, A. F. Nogueira, Ç. Odabaşı, A. Osherov, N.-G. Park, M. O. Reese, F. De Rossi, M. Saliba, U. S. Schubert, H. J. Snaith, S. D. Stranks, W. Tress, P. A. Troshin, V. Turkovic, S. Veenstra, I. Visoly-Fisher, A. Walsh, T. Watson, H. Xie, R. Yıldırım, S. M. Zakeeruddin, K. Zhu and M. Lira-Cantu, Consensus statement for stability assessment and reporting for perovskite photovoltaics based on ISOS procedures, *Nat. Energy*, 2020, **5**(1), 35–49.

101 A. Liu, X. Li, W. Zhang, H. Yang, X. Guo, C. Lu, H. Yuan, W. Ou-Yang and J. Fang, Ag Electrode Anticorrosion in Inverted Perovskite Solar Cells, *Adv. Funct. Mater.*, 2023, **34**(1), 2307310.

102 Y. Kato, L. K. Ono, M. V. Lee, S. Wang, S. R. Raga and Y. Qi, Silver Iodide Formation in Methyl Ammonium Lead Iodide Perovskite Solar Cells with Silver Top Electrodes, *Adv. Mater. Interfaces*, 2015, **2**(13), 1500195.

103 N. Tzoganakis, B. Feng, M. Loizos, K. Chatzimanolis, M. Krassas, D. Tsikritzis, X. Zhuang and E. Kymakis, Performance and Stability Improvement of Inverted Perovskite Solar Cells by Interface Modification of Charge Transport Layers Using an Azulene–Pyridine Molecule, *Energy Technol.*, 2023, **11**(2), 2201017.

104 Q. Xie, C. Hu, L. Xu, L. Chen, W. Wang, H. Yin, G. Cheng and X. Ai, Stability studies of few-layer InSe nanosheets by Raman spectroscopy, *Solid State Commun.*, 2021, **336**, 114417.